1 1 1 1
1

IDENTIFICATION OF GEOLOGICAL STRUCTURE AND ITS IMPACT TO LAND SURFACE TEMPERATURE BASED ON ASTER AND DEM DATA ON "TG14" GEOTHERMAL FIELD, SUMATERA

Aziz Fajar Setiawan, Suharno, Ahmad Zaenudin, Nandi Haerudin
Geophysical Engineering, University of Lampung
azizfajar11@gmail.com

THE 5th INDONESIA INTERNATIONAL GEOTHERMAL CONVENTION & EXHIBITION 2017

Keywords: fault, LST, ASTER, Geothermal, Sumatera

ABSTRACT
In a study of geothermal prospects, the first thing to do is identify the geological conditions in the area. This study aims to determine the geological conditions in the area of "TG14" geothermal field using remote sensing methods on ASTER and DEM imagery and the impact to land surface temperature. The land surface temperature (LST) from thermal infra red (TIR) band using a retrieval method. Surface emissivity was determined based on Normalized Difference Vegetation Index (NDVI) of study area. Remote sensing analysis is good approach to identification of geological structure from surface that control thermal manifestation in "TG14" geothermal field. The hottest temperature in the area along the deep-seated Great Sumatera Fault and the western graben transform fault, heated by magmas associated with the volcanic deposits. It shows Great Sumatera Fault is the main structure in geothermal field which associated with high LST and thermal manifestation.

INTRODUCTION
In a study of geothermal prospects, the first thing to do is identify the geological conditions in the area. "TG14" Geothermal field is located in a major valley and an undulating areas with an altitude ranging from 184 m asl to 1063 m covered by volcanic rock formation. The Semangka valley lies near the southern end of the Sumatra fault zone. The prospects are defined by significant thermal areas which are located near the western margins of the depression.

Quaternary volcanism era dominated Barisan zone, which is represented by 50 volcanic centers along the Sumatra Fault Zone (Sieh and Natawidjaja, 2000). The relationship between volcanism and tectonic activity of the Sumatra Fault are hard to understood, as only a few volcanism which lies on active fault zone, while the majority of them are scattered within 20 to 40 km of the fault zone. It means that the presence of Quaternary volcanism era increasingly more formed to the southeast, a reduced rate because of the shift from Sumatra Fault ductile properties of the magma chamber (Hussein et al, 2015).

Research area is located in Barisan zone consisting of sedimentary and volcanic rocks. The rock formations that make up the "TG14" geothermal area is Alluvium (Qa), Ranau Formation (QTr), Quartenary Volcanic (Qv), Seblat Formation (Toms), Simpangaur Formation (Tmps) and Volcanoes Quarter Young Formation (Qhv). This Volcanic are also basalt and andesite in composition. The area to the north east of The Sumatra Fault Zone is dominated by Young quaternary volcanics (Qhv) which have been erupted from a number of volcanic centers. These are again dominated by basaltic and andesitic rocks but include dacites (Amin et al, 1993).

Thermal remote sensing is based on the measuring of electromagnetic radiation in the infrared region of the spectrum. Most commonly used are the intervals from 3 to 5 µm and 8 to 14 µm, in which the atmospheric absorption. Since the source of the radiation is the heat of the imaged surface itself, the handling and processing of Thermal Infrared (TIR) data is considerably different from remote sensing based on reflected sunlight (Bakker et al, 2009).

This study aims to determine the geological conditions in the area of "TG14" geothermal field using remote sensing methods on ASTER and DEM imagery and the impact to land surface temperature.

DATA
The remote sensing data that used in this research is ASTER image with acquisition date on 27th July 2006 (Day), 6th August 2009 (Night) and 17th October 2011 for ASTER GDEM. All of the data is secondary data downloaded from USGS page. The data used to determine the land surface temperature estimation is the ASTER image of the thermal infrared band and to determine the Normal Different Vegetation Index (NDVI) used band 2 (Red) and band 3 (NIR). While DEM data is used to interpret the lineaments structure automatically.

ASTER image plays a major role in this research where the distribution of land surface temperature is calculated based on the thermals infrared image while the fracture structure is delineated from the automatic lineaments extraction results used as the complementary data of the existence of a new fault in the field which is not shown by the geological map.

METHODS
Structure Geology
Digital lineament extraction was conducted automatically with several parameters such as pixel filter radius, gradation edge limit, curve length limit, differential degree limit and error. The purpose of this analysis was to obtain pattern orientation and distributions based on those parameter. These parameters values were modified from Abdullah (2010).

Table 1 : Extracted Lineament Parameter Values.

Parameter	Value
Filter Radius	12
Edge Gradient Threshold	90
Curve Length Threshold	30
Line Fitting Error Threshold	10
Angular Different Threshold	30
Linking Distance Threshold	20

The extracted lineaments show all possible linear features that can represent lineament pattern. Lineament patterns are used as a parameter to lineament delineation. The accuracy analysis of delineation result of lineaments of faults structure is still qualitatively limited by overlapping and comparing the direction of the main major lineaments with major faults in the geological map of the research area.

Land Surface Temperature
The land surface temperature in the study area was calculated by semi empirical method in which surface emissivity was obtained based on the classification of Normalized Difference Vegetation Index (NDVI) values. The NDVI value itself is obtained by the following algorithm

$$??????? = \frac{??_{nir} - ??_{red}}{??_{nir} + ??_{red}} \quad (1)$$

With $??_{nir}$ and $??_{red}$ is the reflectance of band 3 and band 2.

Land surface temperature obtained from thermal infrared band processing ASTER image that is band 10, 11, 12, 13 and 14. Digital number of each band was first converted into form radiance. The land surface temperature was calculated by the following equation (Ghulam, 2009):

$$?? = \frac{??}{??\left(\frac{??}{??}+1\right)} - 273.15 \quad (2)$$

Therefore, K_1 and K_2 become a coefficient determined by effective wavelength of a satellite sensor. For example, effective wavelength of ASTER band 10, λ=8.291 µm = 8.291×10^{-6} m, we can have $K_1 = C_1/\lambda^5 = 1.19104356\times10^{-16}$ W m^2 / (8.291×10^{-6} m)^5 = 3040136402 W m^{-2} m^{-1} = 3040.136402 W m^2 µm^{-1} $K_2 = C_2/h = 1.43876869\times10^{-2}$ m K / 8.291×10^{-6} m = 1735.337945K. The method may be extended to the rest the ASTER thermal bands as shown in the following table.

Table 2. ASTER thermal bands (Ghulam, 2009).

Bands	Bandpass (µm)	Effective Wavelength (µm)	UCC	K_1 (*)	K_2 (*)
10	8.125-8.475	8.291	0.006882	3040.136402	1735.337945
11	8.475-8.825	8.634	0.006780	2482.375199	1666.398761
12	8.925-9.275	9.075	0.006590	1933.080183	1585.420044
13	10.25-10.95	10.657	0.005693	866.486575	1350.069147
14	10.95-11.65	11.318	0.005225	641.326517	1271.221673

*W m^{-2} µm^{-1}

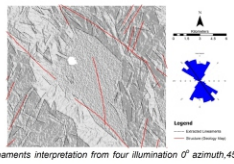

Figure 1. The result of lineaments interpretation from four illumination 0° azimuth,45° azimuth,90° azimuth and 135° azimuth.

Rose Diagram

Statistical Summary	
Calculation Method:	Length
Class Interval:	10.0 Degrees
Min.Length Filtering:	Deactivated
Max.Length Filtering:	Deactivated
Azimuth Filtering:	Deactivated
Data Type:	Bidirectional
Population:	430
Total Length of All Lineations:	14.77
Maximum Bin Population:	50.0
Mean Bin Population:	28.67
Standard Deviation of Bin Population:	16.92
Maximum Bin Population (%):	5.81
Mean Bin Population (%):	3.33
Standard Deviation of Bin Population (%):	1.97
Maximum Bin Length:	0.06
Mean Bin Length:	0.49
Standard Deviation of Bin Lengths:	0.54
Maximum Bin Length (%):	6.61
Mean Bin Length (%):	3.33
Standard Deviation of Bin Lengths (%):	2.29
Vector Mean:	161.9 Degrees
	341.9 Degrees
Confidence Interval:	6.2 Degrees
	[95 Percent]
R-mag:	0.56

Figure 2. Statistical summary of morphological lineament Research area.

From total 430 data, statistic analysis suggests dominant lineament aligned North West – South East following its major faults. This indicates that the main direction of the lineaments of the interpretation results is aligned with the direction of the main structure which also has a North West – South East direction (Sumatera fault system). If associated with the morphology of the study area, the highly steep hilly terrain is where there are higher lineaments structures than the lower morphological units.

The analysis of vegetation on ASTER image results in the appearance of vegetation density on the surface. This analysis uses NDVI method on ASTER image with equation $??????? = \frac{??????? - ???????}{??????? + ???????}$ (Kalinowski and Oliver, 2004). High vegetation density dominates in the peak areas of the hills where as moderate and less-moderate densities are in the middle of the depression area. The peak density is estimated as part of the Bukit Barisan Selatan National Park forest area. While the area of moderate and less-moderate vegetation is estimated as the area of plantation, rice fields and residential communities. The area of manifestation lies in a less vegetation density area and no vegetation, this characterizes the availability of heat alteration minerals.

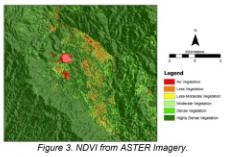

Figure 3. NDVI from ASTER Imagery.

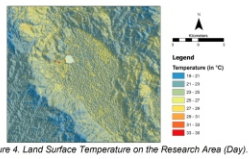

Figure 4. Land Surface Temperature on the Research Area (Day).

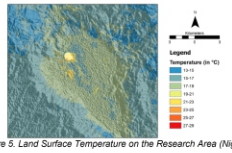

Figure 5. Land Surface Temperature on the Research Area (Night).

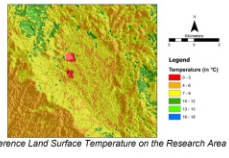

Figure 6. Difference Land Surface Temperature on the Research Area (Day - Night).

Based on Figure 4 and 5, land surface temperature estimation at the focus of the research area is higher in the depressed area compared to the surrounding area with land surface temperature up to 36 °C during the day and 29 °C at night. Then from the all result of land surface temperature estimation is done determination of location having consistent temperature value based on difference between day and night temperature (figure 6). Red color indicates areas that have relatively consistent surface temperatures. Whereas purplish with vegetation density

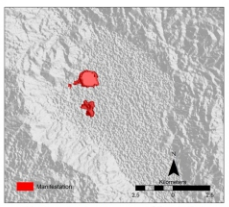

Figure 7. Manifestation Area based on LST and NDVI analysis.

According to Qin et al. (2011) and Wu et al. (2012) that fractures are associated with hot springs and high ground temperatures. Based on the overlay between the fault structure and the land surface temperature in Fig. 8, it is clear that the fault pattern is followed by a fairly high pattern of surface temperature (yellow and orange) and manifestations, so this fault is the main fault of the heat manifestation control of the "TG14" . This condition is due to the distribution of subsurface layers that carry the geothermal manifestation of "TG14" identified to spread following the main fault and river flow pattern that leads to the southeast.

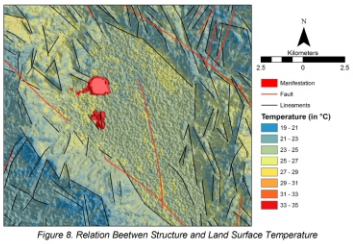

Figure 8. Relation Beetwen Structure and Land Surface Temperature

CONCLUSION
Use of remote sensing data ASTER Imagery and ASTER GDEM can be used to detect new geological structures in the "TG14" area and their effect on land surface temperatures. The results indicate a major fracture as a hot fluid pathway so that it is associated with a high surface temperature. Need to check the data in the field to know the accuracy of the method used. Selection of image data in the research area needs to be done in order to produce quality data.

ACKNOWLEDGEMENT
The author are grateful to thank to USGS for ASTER L1T and ASTER DEM data used in this study.

REFERENCES
Abdullah, A., Juhari, M., A., dan Ibrahim, A., Automatic Mapping of Lineaments Using Shaded Relief Images Derived from Digital Elevation Model (DEMs) in the Maran – Sungi Lembing Area, Malaysia, Electronic Journal of Geophysics Environment Vol. 15, (2010), p.949-957.

Amin, T. C., Sidarto, Santosa, S., Gunawan, W., Geologi/Lembar Kota Agung, Sumatra, Geological Research And Development Center, Bandung, (1993).

Bakker et al, Principles of Remote Sensing, Faculty of Geo-Information Science and Earth Observation, Twente, (2009).

Ghulam, A., How to Calculate Reflectance and Temperature Using ASTER Data, Center for Environmental Sciences, Saint Louis University, (2009).

Husein et al, Tectonic Control to Geothermal System of Way Panas, Lampung, Indonesia, Proceedings World Geothermal Congress 2015, (2015).

Kalinowski, A., and Oliver, S. ASTER Mineral Index Processing Manual. Remote Sensing Applications Geoscience, Australia, 2004.

Qin, Q., Zhang, N., Nan, P., and Chai, L., Geothermal Area Detection using Landsat ETM+ Thermal Infrared Data and its Mechanistic Analysis – A Case Study in Tengchong, China, International Journal of Applied Earth Observation and Geoinformation, (2011) Vol. 13, 552-559.

Sieh, K., Natawidjaja, D., H., Neotectonics of the Sumatran fault, Journal of Geophysical Research, (2000), p.28,295-28,326.

Wu, W., Zou, L., Shen, X., Lu, S., Su, N., Kong, F., and Dong, Y., *Thermal Infrared Remote-Sensing Detection of Thermal Information Associated with Faults: A Case Study in Western Sichuan Basin, China*, Journal of Asian Earth Scienes, (2012), Vol. 43, 110-117.